Effects of molecular-scale processes on observable growth properties of actin networks

J. Zhu* and A. E. Carlsson†
Department of Physics, Washington University, St. Louis, Missouri 63130, USA
(Received 29 October 2009; published 22 March 2010)

The properties of actin network growth against a flat obstacle are studied using several different sets of molecular-level assumptions regarding filament growth and nucleation. These assumptions are incorporated into a multifilament methodology which treats both the distribution of filament orientations and bending of filaments. Three single-filament force-generation mechanisms in the literature are compared within this framework. Each mechanism is treated using two different filament nucleation modes, namely, spontaneous nucleation and branching off pre-existing filaments. We find that the shape of the force-velocity relation depends mainly on the ratio of the thermodynamic and mechanical stall forces of the filaments. If the thermodynamic stall force greatly exceeds the mechanical stall force, the velocity drops abruptly to zero when the mechanical stall force is reached; otherwise, it goes more gradually to zero. In addition, branching nucleation gives a steeper increase in the filament number with opposing force than spontaneous nucleation does. Finally, the zero-force velocity of the obstacle as a function of the detachment and capping rates differs significantly between the different single-filament growth mechanisms. Experiments are proposed to use these differences to discriminate between the network growth models.

DOI: 10.1103/PhysRevE.81.031914 PACS number(s): 87.16.Ka, 87.16.Ln, 87.16.A−

I. INTRODUCTION

In actin-based cellular protrusion and locomotion, mechanical force is generated by the elongation of actin filaments inside the cell. The processes controlling force generation have been studied extensively over the past few decades, and include polymerization, creation of new filaments by branching or spontaneous nucleation, capping, severing, attachment, and detachment [1]. Although these processes are well established in general, the details of the underlying molecular-level mechanisms and the relevant rates are not well understood. For this reason, a number of force-generation models have been developed which differ in their molecular-level assumptions regarding both the single-filament growth mechanism and the mode of nucleation for new filaments.

The single-filament growth mechanisms are of three main types (see Fig. 1).

(1) The tethered ratchet (TR) mechanism [2], which incorporates the earlier Brownian ratchet mechanism [3], assumes that some of the actin filaments are attached to the obstacle. Filaments are created with their barbed ends attached to the obstacle surface. While attached, they do not grow but rather pull the obstacle reactively. After detachment, they polymerize and generate pushing forces similar to those in the Brownian ratchet mechanism. Finally, they become capped and are left behind by the obstacle's motion.

(2) The passive-processive (PP) mechanism [4] assumes that filaments can grow while their barbed ends are attached to the obstacle. For each filament, the attachment point switches thermally between the two terminal subunits, without adenosine triphosphate (ATP) hydrolysis. Actin monomers can attach to the barbed ends if enough space is available between the filament tip and the obstacle. Free filaments provide additional pushing force.

(3) The end-tracking (ET) mechanism [5,6] treats filaments attached to the obstacle surface through a barbed-end tracking protein. The rate with which the tracking protein moves along the filament depends on the filament's ATP hydrolysis rate, and thus growth is coupled to ATP hydrolysis. Therefore, a high protrusion force of up to a few tens of pN is thermodynamically possible. Free filaments can provide an additional smaller pushing force.

These three mechanisms make different predictions for the force-velocity relation of single filaments. In the TR mechanism, the growing filaments follow the exponentially decaying Brownian-ratchet force-velocity relation [3], which is concave up. In the PP mechanism, the force-velocity relation for attached filaments has a sigmoidal shape. The velocity increases to an asymptotic value if a pulling force is present and decreases exponentially for large pushing forces. In the ET mechanism, the velocity of attached filaments remains constant at low force and drops rapidly when the force reaches a threshold, forming a concave-down shape. Due to lack of experimental data on the force-velocity relation of single filaments, the above predictions have not yet been evaluated definitively. A major goal of this work is to evaluate to what extent the differences between the single-filament growth mechanisms persist in more complete models.

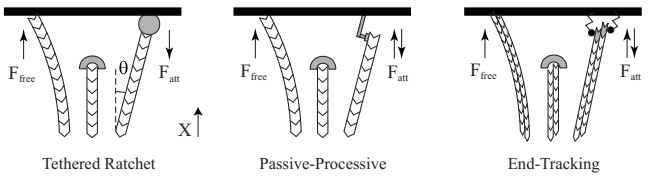

FIG. 1. Three single-filament growth mechanisms. For each mechanism, a free growing filament, a capped free filament, and an attached filament are shown.

*Present address: Department of Mathematics, University of California, Davis, California, USA.
†aec@wustl.edu

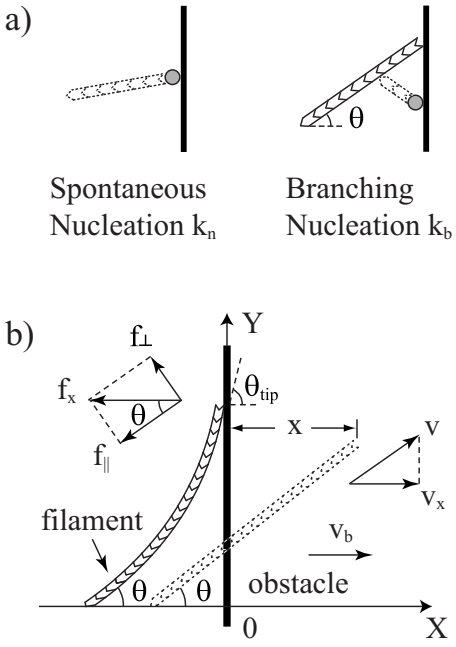

FIG. 2. (a) Filament nucleation modes. Dashed filaments indicate newly created ones. (b) Schematic of a filament pushing against an obstacle, illustrating filament deformation x. Obstacle velocity: v_b. Filament velocity: v. Components of f_x force relative to filament axis are $f_\parallel$ and $f_\perp$. Dotted filament indicates where the filament would have been if there were no obstacle.

The possible modes of filament nucleation are of two main types [see Fig. 2(a)]:

(1) Spontaneous nucleation. Filaments are nucleated near the obstacle surface by proteins such as formins [7]. Preexisting filaments are not required.

(2) Branching nucleation. Filaments are branched from existing filaments in an autocatalytic fashion as would be expected from Arp2/3 complex [8].

Force generation and other properties of actin networks within some combinations of these single-filament growth mechanisms and nucleation modes have been studied theoretically in previous works [2,9–19], incorporating some, but not all, of the effects treated here. However, there has been no comprehensive treatment systematically evaluating the differences between the growth mechanisms and nucleation modes within the context of realistic network growth models.

The combination of three growth mechanisms and two nucleation modes gives altogether six network models. One can of course define many more models by treating additional "fine-tuning" assumptions, but the range of models covered here encompasses most of the existing literature and we address the importance of additional assumptions below. One would like to distinguish between these six models by performing suitable experiments. Measurements of the force-velocity relation [20–24] and the force-filament number relation of actin networks as measured by fluorescence [20,23,24] are in principle promising. Other types of experiments which could be relevant are the dependence of the growth velocity on the concentrations of key actin-binding proteins. It is the purpose of this paper to evaluate the connection between such experimental measurements and the molecular-scale assumptions of the six network models. Thus, we calculate growth properties of the six models taking into account contributions from both free and attached filaments, the distribution of filament orientations, transport of filament tips away from the obstacle, and filament bending. For each model, we calculate the force-velocity relation, the force-filament number relation, and the dependence of the obstacle's zero-force velocity on the filament's capping and detachment rates. We find that the shape of the force-velocity relation depends on the relative magnitudes of the thermodynamic stall force (the opposing force at which polymerization and depolymerization balance for a rigid filament) and mechanical stall force (the force required to bend a filament to be parallel to the obstacle surface). Larger thermodynamic stall forces tend to give force-velocity relations with a sudden drop near the maximum force, while lower thermodynamic forces give a smoother behavior. The mechanical stall force is determined by a "cross-linking distance" l_c. For $l_c=0.2$ μm, we find that the ET mechanism gives a sudden drop, while the TR and PP mechanisms give a smoother behavior. Also, branching nucleation gives a steeper increase in the total number of actin filaments with opposing force than is given by spontaneous nucleation. Finally, the three filament growth mechanisms give different predictions for the capping and detachment rate dependence of the zero-force velocity.

We note that a continuum elastic model [25] based on larger length scales has been used to calculate the force-velocity relation for actin-based propulsion. It treats the actin network as an elastic gel and emphasizes the internal stress instead of the properties of individual filaments. It successfully explained the experimental force-velocity curve for biomimetic beads in a pure-protein solution [20] and explained an actin network instability which cannot be explained by the single-filament growth mechanisms [26]. However, the effects of the single-filament force-velocity relation and the filament nucleation mode on force generation by actin networks have not been explored within this framework.

II. GEOMETRY AND MATHEMATICAL APPROACH

A. Geometry

We treat an actin network polymerizing against a flat rigid obstacle moving in the X direction. The use of a flat obstacle simplifies the connection between the molecular-level assumptions and network growth properties because it reduces the effects of network deformation. The bulk of our calculations are performed using a three-dimensional geometry most relevant to cantilever experiments of the type described by Parekh *et al.* [21]. We feel that the actin gel surface in these experiments is reasonably flat since the filaments are nucleated mainly from the cantilever, rather than the atomic-force-microscopy tip on the cantilever. For concreteness, we take the obstacle to have an area of 180 μm^2 as in Ref. [21]. We also perform a few simulations using a two-dimensional geometry, which is most relevant to the lamellipodial protrusion experiments such as those of Prass *et al.* [22]. For mathematical simplicity, we assume that the actin is stationary and the obstacle moves, but by a simple change in reference

frame these calculations could handle the case of a stationary obstacle and moving actin network. Because we treat a flat obstacle, we do not include shearing deformations of the actin gel. This means that the results are not directly relevant to the propulsion of *Listeria* or protein-coated beads, where such deformations are important [27].

B. Mathematical approach

Our mathematical approach is based on the coarse-grained densities of filaments as a function of their orientation and the local deformation of the actin gel, rather than on stochastic simulation. To motivate our treatment of the local deformation, we note that actin filaments growing at different angles to the substrate will have different X components of the growth velocity. If some of the growing filaments are attached to the obstacle, accommodation of the velocity differences will require local deformation of the actin gel. We treat this effect by allowing the base of each filament to be displaced relative to the surrounding gel. The forces arising from this displacement are described by an effective spring constant k_{el}. The value of k_{el} is determined by the elastic modulus of the actin gel and the average spacing l_c between cross links in the network. As described in Appendix A, we take $k_{\mathrm{el}}(l_c) \approx (l_c/100\ \mathrm{nm})^{-2}\ \mathrm{pN/nm}$. We thus describe the filaments by their orientation θ relative to the X direction and a displacement x which describes the elastic distortion of the gel in the X direction [see Fig. 2(b)]. For a given filament, x is the position that the filament tip would have had relative to the obstacle surface if no force were exerted on the tip. Positive x means that filaments are compressed, and negative x means that filaments are stretched or detached. We denote the corresponding distributions of free and attached filaments by $P_{\mathrm{f}}(x,\theta)$ and $P_{\mathrm{a}}(x,\theta)$. The rates of change in these two distributions depend on the following processes:

Filament nucleation. We assume that new filaments are nucleated in an attached undeformed state, so that $x=0$. Therefore, the rate of change in P_{a} due to filament nucleation can be written as

$$\left.\frac{\partial P_{\mathrm{a}}}{\partial t}\right|_{\mathrm{nuc}} = k_{\mathrm{nuc}}\delta(x), \tag{1}$$

where $k_{\mathrm{nuc}}=k_{\mathrm{nuc}}(\theta)$ is the nucleation rate of filaments with orientation θ as defined below, and $\delta(x)$ is the Dirac delta function. There is also a possibility that new filaments are first created unattached, then attach to the object at a later time. However, we find that the reduction in the number of attached filaments resulting from unattached nucleation can be reproduced by simply changing the attachment rate.

The filament nucleation rate, for either spontaneous or branching nucleation, will depend on the local concentrations of formins or activated Arp2/3 complex. It will also depend strongly on the local free-actin concentration at the obstacle, because the critical nucleus is expected to comprise several monomers [28]. The local concentrations will in general be reduced, because depletion of proteins near the obstacle due to nucleation and filament growth will not be completely compensated by diffusion [29]. The magnitude of the depletion effect is described by reduction factors u_{s} (spontaneous nucleation) and u_{b} (branching nucleation), which are derived in Appendix B. The filament creation rates for the spontaneous and branching nucleation cases are then given by

$$k_{\mathrm{nuc}}(\theta) = \begin{cases} \frac{1}{2}k_{\mathrm{s}}u_{\mathrm{s}}\sin\theta, & \text{spontaneous} \\ k_{\mathrm{b}}u_{\mathrm{b}}\displaystyle\int_{-\pi/2}^{\pi/2} K(\theta,\theta')n_{\mathrm{c}}(\theta')d\theta', & \text{branching,} \end{cases} \tag{2}$$

where k_{s} and k_{b} are the spontaneous and branching nucleation rates without depletion effects, the factor of $\frac{1}{2}\sin\theta$ in the upper equation comes from the range of filament orientations ($-\pi/2$ to $\pi/2$) in spherical coordinates, and $K(\theta,\theta')$ is a three-dimensional branching kernel given by

$$K(\theta,\theta') = \sin\theta/(\pi\sin\theta_{\mathrm{br}}\sin\theta'\sin\phi), \tag{3}$$

where $\theta_{\mathrm{br}}=70°$ is the branching angle and ϕ is an azimuthal angle determined (see Ref. [9]) by θ and θ',

$$\cos\theta = \cos\theta_{\mathrm{br}}\cos\theta' + \sin\theta_{\mathrm{br}}\cos\phi\sin\theta'. \tag{4}$$

To account for the observed spread [8,30] in θ_{br}, we use a weighted integral of the form given by Eq. (4), calculated using a Gaussian distribution of θ_{br} of width $\Delta\theta=10°$. In our two-dimensional calculations, we use a kernel of the form

$$K(\theta,\theta') = \{\exp[-(\theta-\theta'-\theta_{\mathrm{br}})^2/2\Delta\theta^2] + \exp[-(\theta-\theta'+\theta_{\mathrm{br}})^2/2\Delta\theta^2]\}/\sqrt{8\pi}\Delta\theta. \tag{5}$$

In Eq. (2), $n_{\mathrm{c}}(\theta)$ is related to the total number of filaments that are in contact with the obstacle at angle θ,

$$n_{\mathrm{c}}(\theta) = \int_0^\infty [P_{\mathrm{a}}(x,\theta)+P_{\mathrm{f}}(x,\theta)]e^{-f_{\parallel}/f_0}dx + \int_{-\infty}^0 P_{\mathrm{a}}(x,\theta)dx, \tag{6}$$

where $f_{\parallel}=f_{\parallel}(x,\theta)$ is the force along the actin filament (given below), $f_0=k_{\mathrm{B}}T/\delta \approx 1.5$ pN, and $\delta \approx 2.7$ nm is the filament length increment per subunit. The exponential factor describes the reduction in the association rate of branching proteins to the filaments' tips. This force reduction factor is present because the nucleation of a new filament requires insertion of Arp2/3 complex. We do not know the exact magnitude of the force reduction, but for convenience we have assumed the exponential form appropriate for insertional assembly of actin filaments [3].

Capping. We assume that the attached filaments are protected from capping by steric constraints. The rate of change in free filaments from capping is

$$\left.\frac{\partial P_{\mathrm{f}}}{\partial t}\right|_{\mathrm{cap}} = -k_{\mathrm{cap}}P_{\mathrm{f}}, \tag{7}$$

where $k_{\mathrm{cap}}=k_{\mathrm{cap}}(x,\theta)$ is the free filaments' capping rate. Like the branching rate, the capping rate is assumed to be slowed exponentially by opposing force if the filament is in contact with the obstacle. Then

$$k_{\mathrm{cap}}(x,\theta)=\begin{cases}k_c u_c & \text{if } x<0\\ k_c u_c \exp(-f_\parallel/f_0) & \text{if } x\geq 0,\end{cases} \tag{8}$$

where k_c is the barbed capping rate without depletion effects and u_c is the depletion factor for the capping rate (defined similarly to that for the nucleation rate; see Appendix B).

Attachment and detachment. Free and attached filaments can interconvert by attaching to or detaching from the obstacle. We assume that such conversions leave x and θ unchanged. The conversion rates for the free and attached filaments are

$$\left.\frac{\partial P_f}{\partial t}\right|_{\mathrm{conv}}=-k_{\mathrm{att}}P_f+k_{\mathrm{det}}P_a, \tag{9}$$

$$\left.\frac{\partial P_a}{\partial t}\right|_{\mathrm{conv}}=k_{\mathrm{att}}P_f-k_{\mathrm{det}}P_a, \tag{10}$$

where k_{att} is the free filament attachment rate and k_{det} is the detachment rate of attached filaments. We assume that k_{att} is a constant k_a for the free filaments that are in contact with the obstacle,

$$k_{\mathrm{att}}(x)=k_a H(x), \tag{11}$$

where $H(x)$ is the Heaviside step function. We also assume that k_{det} depends on the force in the X direction (see Ref. [2]),

$$k_{\mathrm{det}}(x,\theta)=\begin{cases}k_d & \text{if } x>0\\ k_d \exp(-f_x/f_0) & \text{if } x\leq 0,\end{cases} \tag{12}$$

where k_d is the filament detachment rate in the absence of force and $f_x\leq 0$ is the x component of the force pulling on the filament (see below). Thus, we assume that only pulling forces accelerate detachment. The above formulas apply for the case in which filaments slide freely along the obstacle, which we assume in most of our calculations.

Filament motion relative to obstacle. The rates of change in P_f and P_a due to the motion of filament tips relative to the obstacle are

$$\left.\frac{\partial P_{f,a}}{\partial t}\right|_{\mathrm{motion}}=-\frac{\partial}{\partial x}(v_{f,a}^{\mathrm{rel}}P_{f,a}), \tag{13}$$

where $v_{f,a}^{\mathrm{rel}}$ are the velocities of the attached and free filaments. These are measured in the X direction relative to the obstacle. In order to calculate $v_{f,a}^{\mathrm{rel}}$, we first calculate the force exerted on a filament with filament deformation x. We assume that the force in the X direction follows Hooke's law,

$$f_x=k_{\mathrm{el}}x, \tag{14}$$

where k_{el} (see Appendix A) is the effective spring constant for the base of an actin filament. Then, if $x>0$, $f_x>0$ (pushing force); if $x<0$, $f_x<0$ (pulling force on attached filaments), and $f_x=0$ for filaments not contacting the obstacle.

The magnitude of the force that can be sustained by a filament will be limited by its bending. We thus define a mechanical stall force $f_{\mathrm{mech}}(\theta)$ as the minimum force that will bend a filament with orientation θ to be parallel to the obstacle surface. Since elongation of a filament parallel to the obstacle surface does not contribute to force generation in the X direction, the pushing force of the filament cannot exceed f_{mech}. We assume that f_{mech} also depends on the typical length of filament from the tip to the first anchoring or cross-linking point. We take this length to be the same as the cross-link distance $l_c\approx 0.1-0.2$ μm. Then f_{mech} is approximated as (see Appendix C)

$$f_{\mathrm{mech}}(\theta)\approx\frac{\alpha l_p k_B T}{l_c^2}\left(1-\frac{2|\theta|}{\pi}\right), \tag{15}$$

where $\alpha=3.4$ and $l_p\approx 10$ μm is the persistence length of F actin [31]. The pushing force of an individual filament is thus

$$f_x=\min[k_{\mathrm{el}}x,f_{\mathrm{mech}}(\theta)] \tag{16}$$

for $x>0$. The force component parallel to the filament, which enters its growth rate, is

$$f_\parallel=f_x\cos\theta. \tag{17}$$

The growth velocities of free and attached filaments in the X direction are calculated from these forces as follows. For all three single-filament mechanisms, the free filament velocity has the same form [3],

$$v_f=[v_0 u_v\exp(-f_\parallel/f_0)-v_d]\cos\theta, \tag{18}$$

where v_0 is the free filament barbed-end growth velocity, u_v is the depletion factor for the actin polymerization rate (see Appendix B), and v_d is the depolymerization velocity. The thermodynamic stall force of each free filament is on the scale of f_0, which is consistent with the measured value of a few piconewtons [32], if one assumes that in this experiment only one or two filaments are pushing at a time. For the attached filaments, the growth velocity is given by

$$v_a=\begin{cases}0, & \mathrm{TR}\\ \frac{1}{2}(v_0u_v-v_d)\cos\theta[1-\tanh(f_\parallel/f_0)], & \mathrm{PP}\\ \frac{1}{2}(v_0u_v-v_d)\cos\theta\{1-\tanh[(f_\parallel-f_s)/f_w]\}, & \mathrm{ET}.\end{cases} \tag{19}$$

Note that in the ET mechanism, we have used a tanh function and two parameters $f_w=1.5$ pN and $f_s=8$ pN to approximate the curve obtained via simulation methods [6]. The thermodynamic stall force in this mechanism is much larger than in the other mechanisms since it assumes that hydrolysis is coupled to filament extension. The velocities of the free and attached filaments in the X direction, relative to the obstacle, are

$$v_{f,a}^{\mathrm{rel}}=v_{f,a}\cos\theta-v_b. \tag{20}$$

Total time evolution equation. Using Eqs. (1), (7), (9), (10), and (13), we write a time evolution equation for the two filament populations,

$$\frac{\partial P_{f,a}}{\partial t}=\left.\frac{\partial P_{f,a}}{\partial t}\right|_{\mathrm{nuc}}+\left.\frac{\partial P_{f,a}}{\partial t}\right|_{\mathrm{cap}}+\left.\frac{\partial P_{f,a}}{\partial t}\right|_{\mathrm{conv}}+\left.\frac{\partial P_{f,a}}{\partial t}\right|_{\mathrm{motion}}, \tag{21}$$

so that

TABLE I. Symbol definitions and parameter values.

Symbol	Definition	Value
δ	Half of actin monomer size	2.7 nm
k_a	Free filament attachment rate	1 s^{-1}
k_d	Filament detachment rate at zero force	1 s^{-1}
k_c	Barbed-end capping rate at zero force	0.5 s^{-1}
k_s	Spontaneous nucleation rate on a 180 μm^2 surface	4.5×10^4 s^{-1}
k_b	Branching rate	1.4 s^{-1}
k_{el}	Effective spring constant of actin network	Varies
f_0	Force scale	$k_BT/\delta\approx1.5$ pN
f_{mech}	Filament mechanical stall force	Varies
f_{therm}	Filament thermal stall force	Varies
F_{ext}	External force	Varies
v_0	Free filament growth velocity	70 nm/s
v_b	Obstacle velocity	Varies
v_d	Filament barbed-end depolymerization velocity	3.8 nm/s
l_c	Distance between cross links	0.1–0.2 μm
l_p	Filament persistence length	10 μm

$$\frac{\partial P_f}{\partial t} = -\frac{\partial}{\partial x}(v_f^{rel}P_f) - (k_{att}+k_{cap})P_f + k_{det}P_a, \tag{22}$$

$$\frac{\partial P_a}{\partial t} = -\frac{\partial}{\partial x}(v_a^{rel}P_a) + k_{att}P_f - k_{det}P_a + k_{nuc}\delta(x). \tag{23}$$

Equations (22) and (23) are the bases of our simulations. The parameters are given in Table I, and the justification of their values is given in Appendix D.

C. Simulation procedure

Equations (22) and (23) are solved numerically with a first-order upwind scheme [33]. We use a two-dimensional mesh in the x-θ plane, where θ ranges from 0 to $\pi/2$, and the maximum and minimum values of x are functions of θ. The filament distribution in the range of $-\pi/2\le\theta<0$ can be obtained from symmetry. Defining $x_f^{max}(\theta)$ and $x_a^{max}(\theta)$ to be the solutions to the equations $v_f^{rel}[x_f^{max}(\theta)]=v_a^{rel}[x_a^{max}(\theta)]=0$, the maximum value for x at a given θ is $x_{max}=\max[x_f^{max}(\theta),x_a^{max}(\theta),0]$. The minimum value of x is chosen such that $P_f(x,\theta)$ and $P_a(x,\theta)$ are negligible. For x that is beyond this range, we take $P_f(x,\theta)=P_a(x,\theta)=0$.

To calculate the force-velocity and force-filament number relations, we fix the obstacle velocity and start with distributions P_f and P_a that are concentrated at $x=0$ but uniformly spread out as a function of θ. We then let P_f and P_a evolve until a steady state is reached. The steady state in the simulation is defined as follows: over the time it takes a filament to traverse the entire range of deformation distribution $t\approx x_{max}/v^{rel}$, the variations in F_{tot}, N_f, and N_a are smaller than 1%. At steady state, the external force balances the total force that the filament network exerts on the obstacle in the X direction,

$$F_{ext} = F_{tot} = \int_{-\infty}^{\infty} f_x n_t(x)dx, \tag{24}$$

where $n_t(x)=\int_{-\pi/2}^{\pi/2}[P_f(x,\theta)H(x)+P_a(x,\theta)]d\theta$ is the total number of filaments with deformation x that are in touch with the obstacle and f_x is given by Eq. (16). Here, we assume that the force generation is cooperative among filaments, because in our model filaments have various orientations and do not form parallel bundles. Therefore, the exchange of load-bearing duty [32] is neglected. The numbers of free and attached filaments in the network are

$$N_f = \int_{-\infty}^{\infty}\int_{-\pi/2}^{\pi/2} P_f(x,\theta)d\theta dx, \tag{25}$$

$$N_a = \int_{-\infty}^{\infty}\int_{-\pi/2}^{\pi/2} P_a(x,\theta)d\theta dx, \tag{26}$$

and we define

$$N_{tot} = N_f + N_a. \tag{27}$$

To calculate the zero-force velocity, we use a root finding routine to find the value of v_b at which the total force produced by the actin network at steady state is zero.

We have checked the simulation results against a previous three-dimensional stochastic simulation [9]. As in the stochastic-simulation studies, we take all the filaments to be free and created via autocatalytic branching, and we use the same parameters as in Ref. [9]. We have compared the force-velocity relation and the branching- and capping-rate dependences of the zero-force velocity to those of the stochastic simulations, and the difference between the two approaches is always less than 10%. Thus, our continuum methodology describes the stochastic growth process accurately.

D. Critique of model

The main assumptions and approximations in our calculations are the following:

Treatment of actin network as a homogeneous and isotropic elastic medium. Gardel *et al.* [34] showed that the actin network *in vitro* is homogeneous, isotropic, and elastic over a large range of actin and cross-linker concentrations, in the absence of bundling proteins. Given the rapid kinetics of actin *in vivo*, it is reasonable to make the same assumption in the straight region of a lamellipod. Since we only aim to treat cases where bundling is absent and the size of the obstacle is much larger than the mesh size of the actin network, it is legitimate to treat the actin network as a homogeneous and isotropic elastic medium. A similar assumption has been made in Ref. [26]. If the mesh size of the actin network were comparable to the size of the obstacle, this approximation would no longer be valid.

We also assume that k_{el} is independent of F_{ext}. This is clearly a simplification, because a higher F_{ext} induces a larger N_{tot}, which should lead to a smaller l_c and thus to a higher k_{el}. We find that varying k_{el} in the simulations has very little impact on the force-velocity relation and the force-filament number relation. Therefore, the assumption of constant k_{el} does not affect the validity of our conclusions.

We note that in our elastic-gel model, the possibility of filament polymerization and nucleation being blocked by steric interactions is ignored. The simulations in Ref. [9] included these effects and found them to affect the growth velocity by 10% or less, even at high F-actin densities of 1 mM.

Uniform mechanical stall force. In a real actin network, filaments have varying distances from the tips to the first cross-linking points. The forces required to stall these filament sections via mechanical bending are therefore different. But the filaments are cross linked to the network, and the cross-linking points can yield under external forces. The strongest forces will be felt by the shortest filaments, so this effect will reduce the variations in f_{mech}. Thus, we feel that using a uniform l_c to characterize f_{mech} is legitimate.

We also assume that f_{mech} is independent of F_{ext}. Since F_{ext} probably decreases l_c, as mentioned above, it should increase f_{mech}. If this effect were included in the calculations, filaments would push more effectively at higher F_{ext}, and v_b would decrease more slowly with increasing F_{ext}.

Abrupt bending of filaments. The deflection angle at a filament's tip should increase continuously with the force on the filament, until the filament is parallel to the obstacle's surface or detached. This increase is slow and linear at low forces, but is fast and nonlinear at high forces near f_{mech}. In our calculations, we assume that the filaments keep their orientations at the tip up to the mechanical stall point. This approximation tends to overestimate $f_{\|}$ on the pushing filaments and underestimate $f_{\|}$ on pulling filaments. Therefore, actual filaments could grow faster, and then the actual v_b at a given F_{ext} could be higher than our prediction.

Neglect of change in filaments' orientations. We assume that filaments do not change their pointed-end orientations when forces are exerted on the barbed ends. This is because a single filament can have multiple cross-linking points (with an average spacing of l_c). When a filament is bent at the barbed end, the torque on the filament is distributed among multiple cross-linking points. Therefore, the change in filament orientation itself is small if l_c is small. On the other hand, if l_c is large (greater or comparable to l_p), then the orientation of the filament will undergo significant changes when force is applied to the barbed end of the filament. In this case an angular evolution term should be included in Eqs. (22) and (23). In this work, we assume that l_c is small enough such that the filament's orientation is unchanged by opposing force.

Absence of actin gel flow. The actin network is reported to act like a viscoelastic gel under external forces [35,36]. The effects of the resulting deformation on the v-F relation are not included in our model. For a given external load, the gel's elasticity affects the gel length by allowing compression, and the gel's viscosity affects its growth velocity by allowing compressional flows. One would expect both the extent of compression of the gel and the flow velocity to be proportional to FL/A, where F is the force, L is the length of the gel, and A is its cross-sectional area. Therefore, to experimentally reduce the gel flow and compression effects, one could use a geometry in which the gel length is much smaller than its width. Then it should be legitimate to compare our predicted actin gel growth velocity with experimental observations.

If the elastic compression is not negligible, one way to relate the experimental results to the present theory is to measure the compression ratio of the actin network $\Delta L/L$ by suddenly releasing the external load. Then our predicted v would correspond to the measured v divided by the factor $(1-\Delta L/L)$. To account for viscous flow, one could adjust the measured velocity by subtracting off the compression-flow velocity and then compare this adjusted velocity to our predictions. Using a parallel-dashpot model of the gel, the compression-flow velocity has been estimated to be $v_{flow} \sim FL/\eta_{gel}A$, where η_{gel} is the gel's viscosity [37]. However, these compression effects are probably small in the experiment of Ref. [21], because otherwise the measured velocity would be dropping more rapidly at small forces.

Neglect of lateral forces. One would expect that if filaments are laterally pinned to the obstacle at their attachment points, preventing lateral motion, the resulting forces could impact the growth of the filaments. Therefore, we have performed additional calculations in which filaments are laterally pinned to the obstacle and experience lateral forces f_y. In this case, we assume that a pushing filament can detach only in the Y direction with rate $k_{det}=k_d \exp(|f_y|/f_0)$, and that a pulling filament detaches with rate $k_{det}=k_d \exp(\sqrt{f_x^2+f_y^2}/f_0)$ [see Eq. (12)]. We also assume that, in Eq. (19), the force parallel to a filament is $f_{\|}=f_x \cos\theta+f_y \sin\theta$. As a result, the presence of lateral forces increases both the detachment rate and the opposing force of attached filaments. With an increased detachment rate, the fraction of highly stretched pulling filaments is reduced, and therefore the total pulling force on the obstacle is smaller. On the other hand, with an increased opposing force, the elongation of pushing filaments is reduced, and thus the total pushing force against the obstacle is also smaller. So the net influence of the lateral forces on the balance of total force is limited. Our simulations show

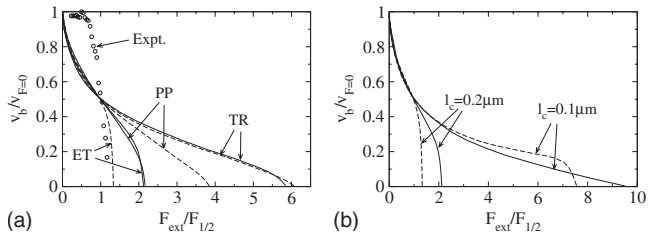

FIG. 3. Force-velocity relation with autocatalytic branching nucleation mode (solid lines) and spontaneous nucleation mode (dashed lines), compared to experimental data from Ref. [21] (Circles). (a) TR, PP, and ET mechanisms with $l_c=0.2$ μm. (b) ET mechanism with $l_c=0.1$ and 0.2 μm.

that the difference between with and without lateral forces in the force-velocity relation is always less than 10%. Thus, in the following calculations, we ignore the effects of lateral forces.

Absence of stochastic effects. At the molecular level, the processes of filament creation, elongation, capping, and detachment are stochastic. Such stochastic effects are not included in our calculations, because we study the network growth properties at a much larger scale, on the basis of averaged properties. As mentioned in the previous section, we have compared our results to those from stochastic simulations [9] and found close agreement. Therefore, the neglect of stochastic effects does not have a major impact on the conclusions.

Absence of filament uncapping. Filament uncapping is not included in our calculations. However, the properties of interest here are mainly determined by the average capping state of the filaments. Therefore, the effects of uncapping would be similar to those of reducing the capping rate.

III. RESULTS

The main outputs of our simulations which could be compared to experiments are the force-velocity relation, the force-filament number relation, and the zero-force velocity's dependence on the detachment and capping rates.

A. Force-velocity relation

Figure 3(a) shows the force-velocity relations for the six network growth models with a cross-link distance of $l_c=0.2$ μm, together with the experimental data from Ref. [21]. $v_{F=0}$ is the obstacle's zero-force velocity and $F_{1/2}$ is the force required to reduce the obstacle's velocity by half. The shapes of the force-velocity relations vary between different models. Both the ET curves, and the PP curve with branching nucleation, display a sharp downturn, while both TR curves, and the PP curve with spontaneous nucleation, give a much more gradual drop. The overall trend seen here is determined by the thermodynamic stall force f_{therm} and the mechanical stall force f_{mech}. In the ET mechanism, f_{therm} is about 11 pN much greater $f_{\text{mech}} \simeq 4$ pN [where f_{therm} is taken to be the value of $f_{\|}$ at $\theta=0$ in Eqs. (18) and (19), for which the filament's growth velocity is reduced to $0.01v_0$]. Therefore, most of the filaments are greatly deflected when F_{ext} reaches a critical value, which gives a steep downturn in the force-velocity relation. On the other hand, in the TR and PP mechanisms, f_{mech} is comparable to the values of f_{therm} of about 4 pN in the TR mechanism and 3 pN in the PP mechanism. Therefore, the filament deflection effect is much smaller, and the force-velocity relation does not show the steep downturn. The reason that PP model with branching nucleation breaks this general trend is that a higher fraction of filaments are in the large θ range than with spontaneous nucleation, so the force required to deflect a filament is much smaller.

The scale of the obstacle velocity also depends on the single-filament growth mechanism. Unfortunately, this difference cannot be a used to distinguish between the mechanisms, because it is sensitive to the choice of parameter values. For example, if most of the filaments in the TR mechanism are free, which corresponds to a high k_d and low k_a, the zero-force velocity can be as high as $(v_0-v_d) \approx 0.95v_0$, close to the value from the ET mechanism. Note also that monomer depletion effects have a large effect on the results for the branching nucleation mode (solid curves). In their absence, v_b is independent of F_{ext}, as found in Ref. [9].

The force-velocity curves for the ET mechanism do not have the same plateau region at low force as found for the single-filament ET mechanism [6]. There are at least two effects that cause this difference. (1) Since F_{tot} contains contributions from a range of filament orientations, there exists a critical angle $\theta_c=\cos^{-1}[v_b/(v_0-v_d)]$ such that all the pushing filaments are in the range of $|\theta|<\theta_c$ [see Eqs. (19) and (20)]. Therefore, at high v_b, θ_c is small, then the number of pushing filaments is small, and v_b is sensitive to the changes in F_{ext}. (2) Filament detachment reduces the average pushing force per filament, especially at high v_b. Each attached filament is created with deformation $x=0$, and x increases with velocity $v_a^{\text{rel}}=v_a \cos\theta - v_b$ toward the maximum deformation $x_a^{\max}$. If k_d is comparable to or higher than $\langle v_a^{\text{rel}} \rangle / x_a^{\max}$, a large fraction of filaments detach and become capped before their deformations reach $x_a^{\max}$. Then the average pushing force per filament is reduced. Thus, at high v_b, F_{tot} is smaller or, equivalently, increasing force reduces v_b. We have checked the importance of the second effect by taking $k_d=0.01$ s^{-1} instead. We find that for small F_{ext}, v_b decreases much more slowly as F_{ext} increases. However, there is still no plateau region in the force-velocity curve, mainly because of the first effect.

Figure 3(a) also compares our simulation results to the experimental data in Ref. [21]. We found that none of the six models are able to reproduce the plateau region in the force-velocity curve observed experimentally. We have tried different parameters in our simulations but found that the shapes of the force-velocity curve remain fairly similar. As an extreme case, we have tried using a step function as the single-filament's force-velocity relation, but we still fail to reproduce the observed behavior. A possible reason is that the actin network in the experiment undergoes a cooperative mechanical instability, as suggested by the observed loading-history dependence [21], which is beyond the scope of our modeling. An alternate possibility is that liquidlike effects of the actin gel are important. A recent model based on these effects [16] reproduced some of the qualitative features seen in the force-velocity curve of Ref. [21].

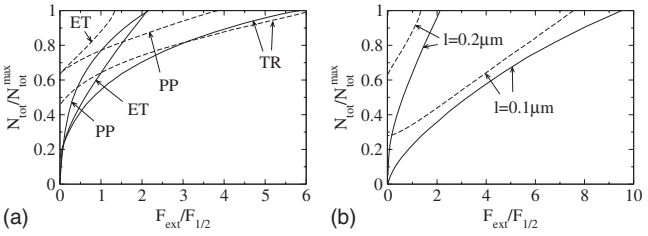

FIG. 4. Force-filament number relation for branching nucleation mode (solid lines) and spontaneous nucleation mode (dashed lines). (a) TR, PP, and ET mechanisms with l_c=0.2 μm. (b) ET mechanism with l_c=0.1 and 0.2 μm.

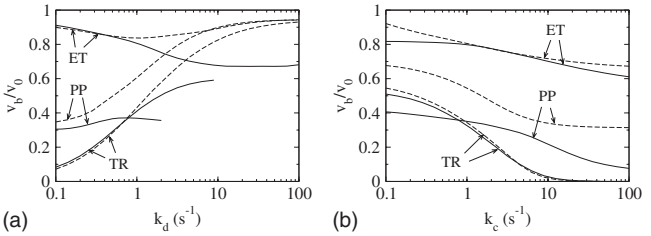

FIG. 5. Zero-force velocity as a function of (a) k_d and (b) k_c, with k_a=1 s^{-1}. TR, PP, and ET mechanisms with both branching nucleation (solid lines) and spontaneous nucleation (dashed lines) are compared.

Figure 3(b) illustrates the effect of mechanical stalling on the force-velocity relation, for the ET mechanism, by varying l_c. At the smaller value of l_c the bend at high forces is reduced or absent. Again the branching and spontaneous nucleation assumptions give very similar force-velocity relations. Similar results are seen for the TR and PP mechanisms. We have tried lower mechanical stall forces in these mechanisms by increasing l_c, and then they develop a sharp downturn similar to that seen in the ET mechanism.

B. Force-filament number relation

Figure 4(a) compares the F_{ext}-N_{tot} relations of the six network models with l_c=0.2 μm. All of the models show N_{tot} increasing with opposing force. Two effects cause this increase. (1) The increased force reduces the filament capping and detachment rates [see Eqs. (8) and (12)] and thus reduces the number of filaments losing their force-generating capacity by capping. (2) The opposing force slows down the obstacle, reducing the number of filaments that are left behind by the obstacle's motion. The first effect is important for spontaneous nucleation since k_s is assumed to be independent of force. It is less important for branching nucleation, because the branching rate is reduced by the external force in a similar fashion as the capping and detachment rates are [see Eqs. (6), (8), and (12)]. The second effect is magnified by branching nucleation, because the creation rate of new filaments is proportional to the number of filaments contacting the obstacle. This leads to a more rapid increase in N_{tot} with F_{ext}. At F_{ext}=0, N_{tot} is lower for branching nucleation than that for spontaneous nucleation. The branching theory [9] predicts that, if all filaments are free, the filament number should vanish in the absence of external force. But with both free and attached filaments, we find that the filament number at zero force is nonzero. This occurs because attached filaments at large angles can produce enough pulling force to balance the pushing force from filaments at small angles.

Figure 4(b) shows that varying l_c also has a moderate effect on the force-filament number relation in the ET model. For the larger value of l_c, in the nucleation branching mode, the growth in N_{tot} is less pronounced than for the smaller value. Similar behavior is seen in the TR and PP models.

C. Dependence of velocity on k_d and k_c

In order to explore further avenues for distinguishing between the network models, we evaluate the k_d and k_c dependences of the zero-force velocity. The k_d dependence displayed in Fig. 5(a) for l_c=0.2 μm shows large differences between different single-filament growth mechanisms. The TR mechanism has the largest change in velocity, and the ET mechanism has the smallest. For the TR and PP mechanisms, increasing k_d causes the obstacle velocity to increase because detached filaments push more effectively. The effect of detachment is much smaller in the ET mechanism because attached filaments push more effectively than free filaments. Therefore, the zero-force velocity is mainly determined by the average zero-force velocity of the attached filaments, which does not depend strongly on the number of attached filaments.

Figure 5(b) shows corresponding results for the k_c dependence of the obstacle's zero-force velocity. The velocity decreases with increased k_c in all six models. However, the extent of the decrease differs strongly between the single-filament growth mechanisms. The TR mechanism has the largest change in velocity; the velocity drops to zero at large k_c. The ET mechanism has the smallest change. For both the k_d and k_c dependences of the zero-force velocity, the branching and spontaneous nucleation modes give very similar results, except that the branching nucleation curves for the PP and TR models terminate earlier as a function of k_d because the filament number becomes very low ($N_{tot}<100$).

IV. DISCUSSION

The above results show that some of the pronounced qualitative differences between the single-filament force-velocity relations of competing growth mechanisms are "washed out" when these mechanisms are embedded in more complete network models. However, observable differences persist in the force-velocity relations and other experimentally accessible quantities. Large values of the thermodynamic stall force f_{therm} in the single-filament growth mechanism tend to produce a sharp concave-down drop in the force-velocity relation. On the other hand, differences in the force-filament number relation are mainly related to differences in filament nucleation mechanism, with branching nucleation giving a sharper climb in the filament number. The capping and detachment-rate dependence of the velocity depend mainly on whether free filaments push more effectively (TR and PP mechanisms) or less effectively (ET mechanism) than attached filaments.

Force-velocity relation. The factor affecting the shape of

the force-velocity relation most is the magnitude of the thermodynamic stall force f_{therm} in comparison with the mechanical stall force f_{mech}. If $f_{\mathrm{therm}} > f_{\mathrm{mech}}$, the force-velocity curve drops rapidly near a critical force per filament around f_{mech}, where many of the filaments begin to be bent. The drop causes a concave-down shape. This effect may be related to the observed sudden drop of obstacle velocity as reported in Refs. [21,22]. However, none of our force-velocity curves reproduce the low-force plateau seen in the experimental data. On the other hand, for $f_{\mathrm{mech}} > f_{\mathrm{therm}}$, filaments can produce strong pushing forces without being significantly bent. This gives the force-velocity curve a concave-up shape.

This prediction could be tested experimentally by varying the cross-linking distance l_c. With decreasing cross-linking protein concentration, l_c will increase and f_{mech} will drop. Therefore, in a force-velocity experiment such as the one in Ref. [21], one should observe a concave-up shape at high cross-linker concentration and a concave-down shape at low cross-linker concentration. The shape of the force-velocity relation will also vary with the free-actin concentration. With increasing free-actin concentration, f_{therm} increases logarithmically [38], so the velocity should develop more of a downward curve. However, increasing actin concentration will also change the mechanical properties of the network, so it is not clear what the net effect would be.

In making the transition from single-filament models to our network model, the ET mechanism undergoes the most significant change in the shape of the force-velocity relation. The reason is that, in the ET mechanism, attached filaments with large angles turn into pulling filaments, which slows down the obstacle especially when the obstacle is moving at a high speed. This makes the force-velocity curve decrease more rapidly with external force near the high velocity region.

For the branching nucleation mode, our model does not have the force-independent protrusion velocity predicted by Ref. [9], because we find that the branching rate is limited by protein concentrations which are limited by diffusion. We have checked that, if the branching rate is kept constant, our network model does give a force-independent protrusion velocity, although it does not reproduce the subsequent drop seen in Ref. [21].

Schaus and Borisy [19] proposed a network model in which a force-velocity curve with a plateau at low forces and a concave-up decay at high forces is produced. The plateau is believed to occur because the velocity is limited by the detachment rate of tethers. The discrepancy between these results and the present ones, however, cannot definitely establish the fundamental difference between their model and ours.

Force-filament number relation. For all six network models, the filament number increases with external force. This occurs because an increased load slows down the obstacle, which in turn decreases the filament capping, detachment, and leaving rates, which increases the number of filaments in contact with the obstacle. Our results also show that the filament number increases more rapidly for the branching nucleation mode. This occurs because the filament creation rate increases with the filament number [11]. Such positive feedback is absent in spontaneous nucleation. As mentioned above, the force-filament number relation could be evaluated by measuring the fluorescence intensity of appropriately labeled actin as a function of force. Analogous measurements of the amount of polymerized actin as a function of time have been made for *Listeria* and actin-propelled beads [20,23,24].

Detachment and capping-rate dependence. For the detachment and capping-rate dependence of the zero-force velocity, there are no significant differences between the branching and spontaneous nucleation modes. However, substantial differences between the three single-filament growth mechanisms exist. Under increases in the detachment rate, the velocity in the TR mechanism changes most, and the velocity in the ET mechanism changes least. Under increases in the capping rate, the velocity in the TR mechanism has the largest change and drops to zero at high capping rates, while the velocity in the ET mechanism has the smallest change and approaches a constant value at high capping rate. We have checked the above trends by assuming that new filaments are created free, and we found similar dependences of the velocity.

A possible way of distinguishing the three single-filament mechanisms experimentally would be to measure the dependence of the zero-force velocity on the detachment rate. One could, for example, add the protein VASP, which appears to increase the filament detachment rate [39–41], to the protein mix used in *in vitro* experiments. Such experiments could use a cantilever setup similar to that of Ref. [21] or freely moving disks as described in Ref. [42]. Existing experiments on beads, to which the present theory is not directly applicable, show that the zero-force speed is enhanced by high VASP levels [39,43–45].

In the types of cells where the flat-lamellipodium approximation is most appropriate, such as migrating keratocytes, VASP can be upregulated or downregulated and the effect on lamellipodial protrusion velocities can be measured. Our two-dimensional calculations show trends very similar to those for the three-dimensional ones. Thus, in either case, one would expect a strong increase in velocity with VASP concentration or activity for the TR mechanism, a modest increase for the PP mechanism, and little variation for the ET mechanism. Measurements of this type have been performed on keratocytes and they give an increase in the velocity with overexpression of VASP [46]. Tentatively these results would speak in favor of the TR or PP mechanisms for keratocytes. Additional experiments with a broader range of cell types would help one to establish the generality of this result.

Measurements of the effects of the capping rate on the zero-force velocity are harder to interpret because capping protein affects the free-actin concentration. Therefore, it is difficult to separate the effect of capping by itself. However, the very strong downturn seen in the TR results should be present regardless of the effects on the free-actin concentration. Thus, if the TR mechanism holds, very large increases in capping protein activity in either *in vivo* or *in vitro* should lead to a slowdown in velocity. Such experiments have not been performed for the geometry treated here, but experiments with *Listeria* [43] indicated that the speed first increases at low capping protein concentrations (presumably

because more monomeric actin becomes available for propulsion) and subsequently decreases at higher concentrations.

ACKNOWLEDGMENTS

We appreciate valuable discussions with David Sept's research group, Philip Bayly, and Frank Brooks. This work was supported by the National Institutes of Health under Grant No. R01-GM086882.

APPENDIX A: ESTIMATE OF k_{el}

By dimensional analysis, one can estimate the spring constant for the displacement of a filament base (which has units of energy/length^2) as $k_{el} \approx E l_c$, where E is the elastic modulus of the actin network and l_c is the distance between cross links. Gardel *et al.* [34] found that $E \propto l_c^{-3}$. Therefore, we take $k_{el} \propto l_c^{-2}$. This is different from the $k_{el} \propto l_c^{-3}$ scaling for the bending constant of a clamped filament as obtained in Refs. [6,47], because we include the motion of the filament base in the background of the network. By growing actin networks around beads in cell extracts, Plastino *et al.* [48] found that for an actin network with an elastic modulus of 10^4 Pa induced by the protein ActA, the mesh size is about 50 nm. We take $l_c = 100$ nm as an estimate for the cross-link distance in this experiment. Therefore, the spring constant of the network for this l_c is $k_{el} \approx 10^4$ Pa $\times$ 100 nm $= 1$ pN/nm. For other values of l_c, the l_c^{-2} scaling implies that $k_{el}(l_c) \approx (l_c/100 \text{ nm})^{-2}$ pN/nm.

APPENDIX B: CALCULATION OF u_v, u_c, u_b, AND u_s

The recruitment rates of actin monomers, capping protein, and Arp2/3 complex are limited by the depletion of free proteins in the polymerization zone. Therefore, as the rate of actin monomer consumption or the density of actin filaments increases, the growth, capping, and nucleation rates may decrease. Dickinson and Purich [29] estimated that, near a biomimetic bead, the slowing of polymerization due to monomer depletion satisfies

$$u_v = [G]/[G]_\infty \approx (1 + N k_B^+/4\pi DR)^{-1}, \tag{B1}$$

where N is the number of growing filaments ($N = N_f$ for the TR model; $N = N_{tot}$ for the ET and PP models), k_B^+ is the barbed-end monomer on-rate constant as mentioned before, D is the monomer diffusion constant, and R is the bead's radius; the first equality holds since the on rate is proportional to the monomer concentration. The geometry treated in the cantilever experiments [21] is a flat surface, roughly rectangular, of area approximately 180 μm^2 (visually estimated in Fig. 1 of the paper). The diffusion calculation is considerably more complex for this geometry than for a sphere. For this reason, and because our calculations do not aim for quantitative accuracy, we obtain our depletion coefficients by performing a calculation for a sphere of area 180 μm^2, so that in Eq. (B1) $R = 3.8$ μm. In addition, we take $D = 4$ μm^2/s [49,50].

To calculate u_c, we note that the intracellular concentration of capping protein is typically about one to two orders of magnitude lower than the G-actin concentration [51]. On the other hand, for a typical filament length of 0.1–0.3 μm, there are 30–100 subunits per filament. If we assume that all filaments eventually become capped, this means that the consumption rate of capping protein will be lower than that of actin by a factor equal to the filament length. Therefore, the depletion factors should be similar in magnitude, and we take $u_c = u_v$.

For branching nucleation, k_b depends on both the free-actin monomer concentration $[G]$ and the Arp2/3 concentration [Arp2/3]. Carlsson *et al.* [28] estimated $k_b \propto [G]^2$ [Arp2/3] from a fit to polymerization dynamics, which corresponds to a critical nucleus of one Arp2/3 complex and two actin monomers. In cells, the ratio of free Arp2/3 complex to G actin is usually on the same order of magnitude as that of capping protein [51]. If we assume, as for capping protein, that one Arp2/3 complex is used for every filament, it is then reasonable to assume that the depletion factor for Arp2/3 complex is the same as that for G actin. Therefore, since the branching rate contains one factor of the Arp2/3 complex concentration and two factors of the G-actin concentration, we take

$$u_b = u_v^3 \approx (1 + N k_B^+/4\pi DR)^{-3}. \tag{B2}$$

Assuming that spontaneous nucleation involves a critical nucleus of size similar to that for branching, we take $u_s = u_b$.

APPENDIX C: CALCULATION OF f_{mech}

The geometry of a filament pushing against a surface is shown in Fig. 2. We define the angle between the filament and the X direction at the pointed end to be θ, and the angle at the barbed end to be θ_{tip}. We assume that the pointed end of the filament is clamped and that the barbed end can move freely along the surface. Therefore, θ is independent of force and θ_{tip} increases with the pushing force f_x. Dickinson *et al.* [6] showed that for such a filament, the force satisfies

$$f_x = \frac{l_p k_B T}{l^2}\left[K\left(\sin\frac{\theta_{tip}}{2}\right) - F\left(\phi_0, \sin\frac{\theta_{tip}}{2}\right)\right]^2, \tag{C1}$$

where $\phi_0 = \sin^{-1}[\sin(\theta/2)/\sin(\theta_{tip}/2)]$; $K(k)$ and $F(z,k)$ are the complete and incomplete elliptic integrals of the first kind, respectively. We define $f_{mech}(\theta)$ to be the force in the X direction that gives $\theta_{tip} = \pi/2$, at which filament can no longer produce pushing forces. We have evaluated $f_{mech}(\theta)$ numerically and find that a linear relation between $f_{mech}(0) = l_p k_B T K^2(1/\sqrt{2})/l^2 \approx 3.4 l_p k_B T/l^2$ and $f_{mech}(\pi/2) = 0$ gives a very good fit. Therefore, we use this linear approximation to calculate $f_{mech}(\theta)$ in Eq. (15).

APPENDIX D: CHOICE OF PARAMETERS

To our knowledge, there are no definitive experimental measurements of the attachment rate k_a or the detachment rate k_d. To obtain a very rough estimate of k_a, we calculate the first-passage time $1/k_a$ for a filament to reach a binding site. We take the spacing between the binding sites to be

$d=17$ nm [48] and the radius of a binding site to be $r_b=0.5$ nm. This radius represents not the size of the protein to which the tip binds, but rather the displacement from the optimal binding position which is required to reduce binding substantially. The filament tip is treated as a freely diffusing particle moving on the obstacle surface. Once it touches a binding site, it becomes attached. To estimate the first-passage time, we evaluate the first-passage time $w(r)$ for a particle diffusing from an outer circle with radius $d/2$ to an inner circle with radius r_b. This time satisfies $w''(r)+w'(r)/r=-1/D_{tip}$, with boundary condition $w(r_b)=w'(d/2)=0$, where D_{tip} is the diffusion constant of the filament tip [52]. Then a simple calculation shows that $w(d/2)=d^2\ln(d/2r_b)/8D_{tip}-(d^2/4-r_b^2)/4D_{tip}$. The value of D_{tip} has been calculated using a normal-mode analysis [53]. For a filament with length $l=200$ nm, a lowest-mode approximation gives $D_{tip}=4D\delta/l\approx 0.2$ $\mu m^2/s$, where $D\approx 4$ $\mu m^2/s$ is the diffusion constant of an actin monomer [49,50] and $\delta=2.7$ nm is the filament length increment per actin subunit. Then $k_a\approx 1/w(d/2)\approx 6000$ s^{-1}.

Literature estimates of k_d vary widely. In a study of actin propelled beads [54], a few filaments about 1 μm in length were observed to be attached to submicron beads. Evaluation of the time that it would take a filament to grow to this length suggests a detachment rate on the order of 1 s^{-1} or less. On the other hand, Vavylonis *et al.* [55] estimated the profilin–barbed-end dissociation rate to be 2500 s^{-1}. If the interaction between the filaments and the obstacle in our study is similar to that between filaments and profilin, then the value of k_d could be as high. Since there are no accurate measurements of k_a or k_d, we have evaluated the effects of a broad range of variation of these parameters on our results. Varying k_d from 1 to 2500 s^{-1}, we find that the results are determined mainly by the ratio of k_a to k_d. Therefore, our strategy for fixing k_a and k_d is to use base line values of 1 s^{-1}, which lead to numerically tractable calculations, and subsequently to evaluate the effects of deviations from these base line values.

We take the maximum polymerization velocity to be $v_0=70$ nm/s, which—using an on-rate constant of 11.6 μM^{-1} s^{-1} [56]—corresponds to a free monomer concentration of $G=2-3$ μM, similar to the typical *in vitro* concentrations [57]. The actin filament depolymerization velocity is $v_d=k_B^-\delta\approx 3.8$ nm/s, where $k_B^-\approx 1.4$ s^{-1} is the barbed-end depolymerization rate of ATP actin [56].

The on rate of capping protein to the barbed end of actin filaments has been estimated to be $k_{cap}^{B,+}=3-8$ μM^{-1} s^{-1} [28,58]. Here, we take $k_{cap}^{B,+}=5$ μM^{-1} s^{-1} and assume the concentration of capping protein to be $[CP]=0.1$ μM, an intermediate value between *in vivo* [51] and *in vitro* [43,57] estimates. Then the capping rate in the absence of depletion effects is $k_c=k_{cap}^{B,+}[CP]\approx 0.5$ s^{-1}.

The spontaneous nucleation rate k_s is estimated as follows. At steady state, the rate of filament creation should be equal to the rate of filament extinction. Since extinction in our model results only from capping, k_s satisfies

$$k_s=\int_{-\infty}^{\infty}\int_{-\pi/2}^{\pi/2}k_{cap}(x,\theta)P_f(x,\theta)d\theta dx\le k_cN_f\le k_cN_{tot}, \tag{D1}$$

where N_f is the total number of free filaments and N_{tot} is the total number of free and attached filaments. For concreteness we take the area to be 180 μm^2 (see Appendix B). We thus estimate the maximum value of N_{tot}, corresponding to a density of 1000 μm^{-2} [59], to be $N_{tot}^{max}=1.8\times 10^5$. Then the upper limit of k_s is $k_s^{max}=k_cN_{tot}^{max}\approx 9\times 10^4$ s^{-1}, and we use an intermediate value of $k_s=4.5\times 10^4$ s^{-1}. The branching nucleation rate k_b is estimated from a filament branch spacing of $l_b\approx 50$ nm [30]. Using the maximum polymerization velocity given above, we obtain $k_b=v_0/l_b\approx 1.4$ s^{-1}.

[1] T. D. Pollard and G. G. Borisy, Cell **112**, 453 (2003).
[2] A. Mogilner and G. Oster, Biophys. J. **84**, 1591 (2003).
[3] C. S. Peskin, G. M. Odell, and G. F. Oster, Biophys. J. **65**, 316 (1993).
[4] J. Zhu and A. E. Carlsson, Eur. Phys. J. E **21**, 209 (2006).
[5] R. B. Dickinson and D. L. Purich, Biophys. J. **82**, 605 (2002).
[6] R. B. Dickinson, L. Caro, and D. L. Purich, Biophys. J. **87**, 2838 (2004).
[7] D. R. Kovar and T. D. Pollard, Proc. Natl. Acad. Sci. U.S.A. **101**, 14725 (2004).
[8] R. D. Mullins, J. A. Heuser, and T. D. Pollard, Proc. Natl. Acad. Sci. U.S.A. **95**, 6181 (1998).
[9] A. E. Carlsson, Biophys. J. **81**, 1907 (2001).
[10] A. Mogilner and L. Edelstein-Keshet, Biophys. J. **83**, 1237 (2002).
[11] A. E. Carlsson, Biophys. J. **84**, 2907 (2003).
[12] J. B. Alberts and G. M. Odell, PLoS Biol. **2**, e412 (2004).
[13] E. Atilgan, D. Wirtz, and S. X. Sun, Biophys. J. **89**, 3589 (2005).
[14] T. E. Schaus, E. W. Taylor, and G. G. Borisy, Proc. Natl. Acad. Sci. U.S.A. **104**, 7086 (2007).
[15] N. J. Burroughs and D. Marenduzzo, Phys. Rev. Lett. **98**, 238302 (2007).
[16] K.-C. Lee and A. J. Liu, Biophys. J. **97**, 1295 (2009).
[17] K.-C. Lee and A. J. Liu, Biophys. J. **95**, 4529 (2008).
[18] F. Huber, J. Käs, and B. Stuhrmann, Biophys. J. **95**, 5508 (2008).
[19] T. E. Schaus and G. G. Borisy, Biophys. J. **95**, 1393 (2008).
[20] Y. Marcy, J. Prost, M.-F. Carlier, and C. Sykes, Proc. Natl. Acad. Sci. U.S.A. **101**, 5992 (2004).
[21] S. H. Parekh, O. Chaudhuri, J. A. Theriot, and D. A. Fletcher, Nat. Cell Biol. **7**, 1219 (2005).
[22] M. Prass, K. Jacobson, A. Mogilner, and M. Radmacher, J. Cell Biol. **174**, 767 (2006).
[23] S. Wiesner, E. Helfer, D. Didry, G. Ducouret, F. Lafuma, M.-F. Carlier, and D. Pantaloni, J. Cell Biol. **160**, 387 (2003).
[24] J. L. McGrath, N. J. Eungdamrong, C. I. Fisher, F. Peng, L. Mahadevan, T. J. Mitchison, and S. C. Kuo, Curr. Biol. **13**,

329 (2003).
[25] J. Prost, *Physics of Bio-Molecules and Cells*, Les Houches Summer School (Springer, Berlin, 2002), pp. 215–236.
[26] F. Gerbal, P. Chaikin, Y. Rabin, and J. Prost, Biophys. J. **79**, 2259 (2000).
[27] E. Paluch, J. van der Gucht, J.-F. Joanny, and C. Sykes, Biophys. J. **91**, 3113 (2006).
[28] A. E. Carlsson, M. A. Wear, and J. A. Cooper, Biophys. J. **86**, 1074 (2004).
[29] R. B. Dickinson and D. L. Purich, Biophys. J. **91**, 1548 (2006).
[30] T. M. Svitkina and G. G. Borisy, J. Cell Biol. **145**, 1009 (1999).
[31] H. Isambert, P. Venier, A. C. Maggs, A. Fattoum, R. Kassab, D. Pantaloni, and M.-F. Carlier, J. Biol. Chem. **270**, 11437 (1995).
[32] M. J. Footer, J. W. J. Kerssemakers, J. A. Theriot, and M. Dogterom, Proc. Natl. Acad. Sci. U.S.A. **104**, 2181 (2007).
[33] W. H. Press, B. P. Flannery, S. A. Teukolsky, and W. T. Vetterling, *Numerical Recipes in C*, 2nd ed. (Cambridge University Press, Cambridge, England, 1992).
[34] M. L. Gardel, J. H. Shin, F. C. MacKintosh, L. Mahadevan, P. Matsudaira, and D. A. Weitz, Science **304**, 1301 (2004).
[35] M. L. Gardel, J. H. Shin, F. C. MacKintosh, L. Mahadevan, P. A. Matsudaira, and D. A. Weitz, Phys. Rev. Lett. **93**, 188102 (2004).
[36] K. O. Okeyo, T. Adachi, J. Sunaga, and M. Hojo, J. Biomech. **42**, 2540 (2009).
[37] F. Jülicher, K. Kruse, J. Prost, and J.-F. Joanny, Phys. Rep. **449**, 3 (2007).
[38] T. L. Hill and M. W. Kirschner, Int. Rev. Cytol. **78**, 1 (1982).
[39] S. Samarin, S. Romero, C. Kocks, D. Didry, D. Pantaloni, and M.-F. Carlier, J. Cell Biol. **163**, 131 (2003).
[40] J. Plastino, S. Olivier, and C. Sykes, Curr. Biol. **14**, 1766 (2004).
[41] L. Trichet, O. Campàs, C. Sykes, and J. Plastino, Biophys. J. **92**, 1081 (2007).
[42] I. M. Schwartz, M. Ehrenberg, M. Bindschadler, and J. L. McGrath, Curr. Biol. **14**, 1094 (2004).
[43] T. P. Loisel, R. Boujemaa, D. Pantaloni, and M.-F. Carlier, Nature (London) **401**, 613 (1999).
[44] V. Laurent, T. P. Loisel, B. Harbeck, A. Wehman, L. Gröbe, B. M. Jockusch, J. Wehland, F. B. Gertler, and M.-F. Carlier, J. Cell Biol. **144**, 1245 (1999).
[45] M. Geese, J. J. Loureiro, J. E. Bear, J. Wehland, F. B. Gertler, and A. S. Sechi, Mol. Biol. Cell **13**, 2383 (2002).
[46] C. I. Lacayo, Z. Pincus, M. M. VanDuijn, C. A. Wilson, D. A. Fletcher, F. B. Gertler, A. Mogilner, and J. A. Theriot, PLoS Biol. **5**, e233 (2007).
[47] A. Mogilner and G. Oster, Biophys. J. **71**, 3030 (1996).
[48] J. Plastino, I. Lelidis, J. Prost, and C. Sykes, Eur. Biophys. J. **33**, 310 (2004).
[49] V. C. Abraham, V. Krishnamurthi, D. L. Taylor, and F. Lanni, Biophys. J. **77**, 1721 (1999).
[50] F. Lanni and B. R. Ware, Biophys. J. **46**, 97 (1984).
[51] T. D. Pollard, L. Blanchoin, and R. D. Mullins, Annu. Rev. Biophys. Biomol. Struct. **29**, 545 (2000).
[52] N. G. van Kampen, *Stochastic Processes in Physics and Chemistry* (North-Holland Publishers, New York, 1992).
[53] L. Yang, D. Sept, and A. E. Carlsson, Phys. Rev. E **76**, 021911 (2007).
[54] L. A. Cameron, T. M. Svitkina, D. Vignjevic, J. A. Theriot, and G. G. Borisy, Curr. Biol. **11**, 130 (2001).
[55] D. Vavylonis, D. R. Kovar, B. O'Shaughnessy, and T. D. Pollard, Mol. Cell **21**, 455 (2006).
[56] T. D. Pollard, J. Cell Biol. **103**, 2747 (1986).
[57] O. Akin and R. D. Mullins, Cell **133**, 841 (2008).
[58] D. A. Schafer, P. B. Jennings, and J. A. Cooper, J. Cell Biol. **135**, 169 (1996).
[59] A. Upadhyaya, J. R. Chabot, A. Andreeva, A. Samadani, and A. van Oudenaarden, Proc. Natl. Acad. Sci. U.S.A. **100**, 4521 (2003).